

YbNiSi₃: An antiferromagnetic Kondo lattice with strong exchange interaction

M. A. Avila, M. Sera, and T. Takabatake

Department of Quantum Matter, ADSM, Hiroshima University, Higashi-Hiroshima 739-8530, Japan

(Received 20 July 2004; published 30 September 2004)

We report on the structural, thermodynamic, and transport properties of high quality single crystals of YbNiSi₃ grown by the flux method. This compound crystallizes in the SmNiGe₃ layered structure type of the *Cmmm* space group. The general physical behavior is that of a Kondo lattice showing an antiferromagnetic ground state below $T_N=5.1$ K. This is among the highest ordering temperatures for a Yb-based intermetallic, indicating strong exchange interaction between the Yb ions, which are in or very close to +3 valency based on the effective moment of $4.45\mu_B/\text{f.u.}$ The compound has moderately heavy-electron behavior with a Sommerfeld coefficient of 190 mJ/mol K^2 . Resistivity is highly anisotropic and for $I \perp b$ exhibits the signature logarithmic increase below a local minimum, followed by a sharp decrease in the coherent/magnetically ordered state, resulting in a residual resistivity of $1.5 \mu\Omega \text{ cm}$ and a residual resistivity ratio of 40. Fermi-liquid behavior consistent with a ground-state doublet is clearly observed below 1 K.

DOI: 10.1103/PhysRevB.70.100409

PACS number(s): 75.30.Mb, 72.15.Qm, 75.20.Hr, 71.27.+a

Ytterbium compounds continue to be a subject of great interest due to the variety of unusual physical properties they can present, in general, associated with the fact that this element's f^{13} and f^{14} electronic states are very close in energy, and also hybridize easily with the conduction band. As a consequence, Yb-based compounds can display mixed valency, heavy fermion, and Kondo lattice characteristics, which provide opportunities for better understanding the physics of such phenomena. In this sense, Yb is often regarded as the “hole” equivalent of Ce, whose f^0 and f^1 states display the same characteristics, but the latter's compounds are by far the most explored among these two rare earths, in many cases simply because the Yb-based compounds bear the “stigma” of being considered more difficult to synthesize.¹

The RTX_3 family of intermetallics (R =rare earth; T =transition metal; X =Si, Ge) is one such case. Many of the Ce-based compounds in the family have been synthesized and extensively investigated over the past decade or so,^{2–8} but practically nothing has been reported so far on heavy rare-earth (R =Tb–Lu) members of these series^{9,10} and, in particular, for R =Yb. We thus thought it would be worth initiating such a line of research and here report on our first results for the title compound.

Single crystals of YbNiSi₃ were grown from Sn flux¹¹ using a starting proportion of 1:1:3:20. The high-purity elements (Yb: Ames Laboratory) were loaded and sealed inside an evacuated quartz ampoule, which was then heated to 1150°C and slowly cooled to 500°C , at which point the ampoule was removed from the furnace and most of the excess flux was separated by decanting. The crystals have excellent resistance to acid and can be left in a pure HCl bath for as long as necessary to remove any remaining flux droplets from the surface. The resulting crystals are platelike, with the main surface orthogonal to the crystallographic b direction, as evidenced from the surface x-ray diffraction (XRD) pattern shown in Fig. 1(a) which has only $(0k0)$ reflections. The largest crystal plates were limited mostly by the ampoule wall itself, but the best crystals—those that

grew compact, isolated, with smooth surfaces and straight edges—have lengths up to 5 mm and thicknesses up to 0.3 mm. Many of the crystals display some interesting, rectangular surface topology patterns resulting from the particular flux-growth dynamics of this compound. Electron-probe microanalysis (EPMA) confirmed the stoichiometric 1:1:3 proportion in the crystals and found the Sn inclusions to be less than 0.03%. Our attempts to grow nonmagnetic YNiSi₃ and LuNiSi₃ crystals by the same method were unsuccessful, so the phase diagram seems to be particularly favorable for R =Yb.

Figure 1(b) shows the XRD pattern of crystals that were crushed into a fine powder. The pattern is consistent with the *Cmmm* space group of the SmNiGe₃ structure-type shown in Fig. 1(c), which has close values for the a and c unit-cell parameters and a layered structure along the b axis. A Rietveld refinement of this spectrum resulted in $a=3.8915(1)$, $b=20.8570(6)$, $c=3.9004(1)$, and $V=316.58 \text{ \AA}^3$. The crystals' platelike morphology described above is therefore consistent with the general observation that the macroscopic dimensions of flux-grown crystals often have an inverse relation to the microscopic lattice parameters. A more detailed structural study will be required though, in order to determine the exact atomic positions in the unit cell of YbNiSi₃.

As one might expect from the layered structure of YbNiSi₃, the electrical resistivity below room temperature is anisotropic as shown in Fig. 2(a). For $I \perp b$ the behavior is metallic, with room-temperature resistivity of about $60 \mu\Omega \text{ cm}$, which initially decreases on cooling, reaches a local minimum centered at 55 K, then increases again until reaching a peak at 7 K. Below this temperature it begins to decrease very fast. A peak in dp/dT places the maximum slope of this drop at 5.0 K, which we will later show to be associated with the Neél temperature T_N of the antiferromagnetically ordered Yb moments, and therefore the strong decrease as a whole can be understood as a combined effect of magnetic ordering at T_N with the onset of coherent scattering of the hybridized Yb moments below $T \sim 7$ K. Figure 2(b)

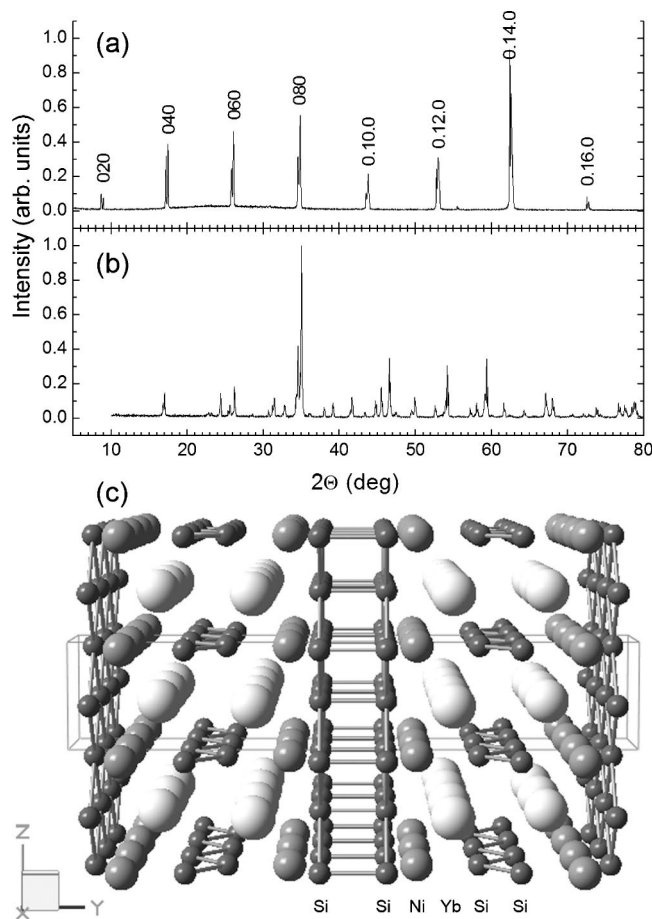


FIG. 1. (a) XRD ($\text{Cu } K\alpha$) pattern of a platelike crystal surface, revealing only the $(0k0)$ reflections. (b) XRD pattern of YbNiSi_3 crystals ground to a fine powder, showing the full set of Bragg reflections. (c) Schematic representation of the atomic positions showing the unit cell (solid line) and layered structure along the b axis.

shows the $I \perp b$ resistivity plotted against $\log T$, where a logarithmic behavior is seen between the local minimum and the peak, a signature of the Kondo effect. The inset of Fig. 2(b) details the resistivity behavior well below the transition, plotted against T^2 . A Fermi-liquid-type $\rho = \rho_0 + AT^2$ behavior is clearly observed below 1 K, with $\rho_0 = 1.5 \mu\Omega \text{ cm}$ and $A = 0.36 \mu\Omega \text{ cm/K}^2$. The residual resistivity ratio (RRR) defined as $\rho(300 \text{ K})/\rho_0$ is 40. These results attest to the clean metallic character and high crystallographic quality of the sample.

The resistivity measurements with $I \parallel b$, shown in Fig. 2(a), were made rather difficult by the fact that the crystals do not grow large in this direction and we were only able to place four contacts on a crystal cut to form a rather irregularly shaped bar along the b axis. Therefore, the estimate of the sample cross section may contain errors of a factor of 2 or even more. Still, it is likely that in this direction the resistivity level is significantly higher than for $I \perp b$ and the temperature dependence resembles that of a semimetal, initially almost flat and then increasing down to the transition temperature. This change in qualitative behavior may be a manifestation of a strongly anisotropic Fermi-surface resultant

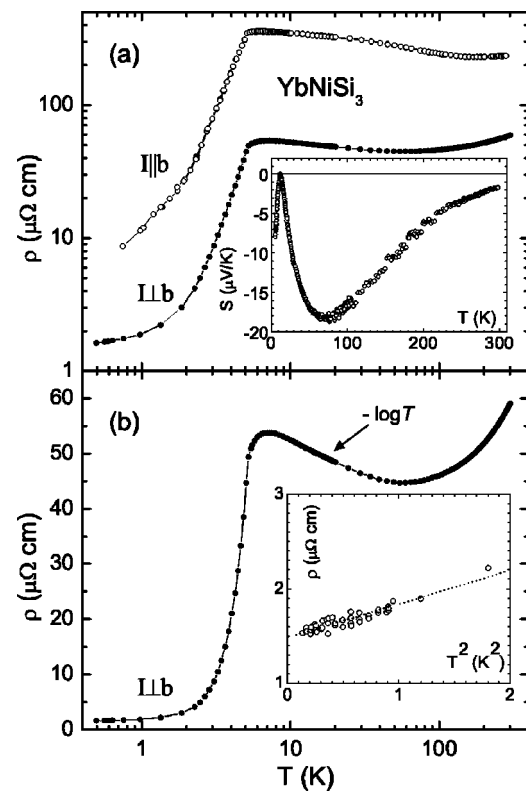


FIG. 2. (a) Anisotropic electrical resistivity $\rho(T)$ of YbNiSi_3 below room temperature. The inset shows the thermopower $S(T)$. (b) $\log T$ dependence of $\rho(T)$ for $I \parallel b$. The inset shows the T^2 dependence of $\rho(T)$ at temperatures below 1 K.

from the layered structure, since in this direction the conduction band crosses tightly bound Si double layers as shown in Fig. 1(c).

The inset of Fig. 2(a) shows the measured thermopower $S(T)$. As for many Yb compounds, $S(T)$ is negative and shows a broad minimum below room temperature. The minimum is located at 72 K and reaches a value of $S = -19 \mu\text{V/K}$. Below this temperature it increases again, reaches a peak very close to $S = 0$ at 12 K, and from there $S(T)$ starts decreasing fast again. Since it is expected to vanish at $T = 0$ we can deduce that a second minimum exists. The peak at 12 K places YbNiSi_3 in the crossover region between compounds where Yb is essentially +3 and such a peak enters the positive side of $S(T)$, and compounds where Yb displays mixed valency behavior and this peak is either well into the negative region or simply does not exist.^{12,13}

The magnetic behavior is also anisotropic, since the crystal electric field (CEF) environment at the Yb site splits the $4f$ multiplet into nondegenerate electronic energy levels. Well above the magnetic ordering temperature, the inverse susceptibility $\chi^{-1}(T)$ for $B = 0.1 \text{ T}$ is typical of paramagnetic local moments with CEF effects (Fig. 3). The $\chi^{-1}(T)$ curves for $\mathbf{B} \parallel b$ and $\mathbf{B} \perp b$ are essentially linear and parallel to each other, and the easy alignment direction for the Yb moments is towards the b direction. As the temperature decreases below 50 K the two curves deviate strongly from Curie-Weiss behavior, while the polycrystalline average estimated as $\chi_p^{-1} = 3/(\chi_b + 2\chi_{ac})$ (dotted line), which should average out

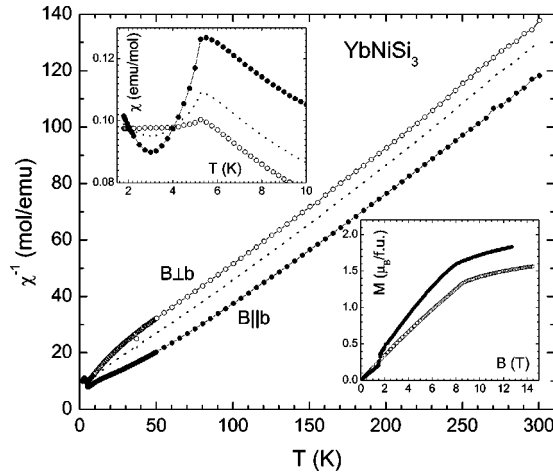


FIG. 3. Anisotropic magnetic behavior of YbNiSi₃. Solid symbols are for $B \parallel b$, open symbols are for $B \perp b$, and dotted lines are the polycrystalline averages. Main plot: temperature dependence of the inverse susceptibility at $B=0.1$ T, showing Curie-Weiss behavior at high temperatures. Upper inset: detail of the antiferromagnetic transition at $T_N=5.1$ K appearing in susceptibility. Lower inset: magnetization isotherms at $T=2$ K, revealing a spin-flop transition at 1.7 T for $B \parallel b$.

the CEF effects assuming that any existing anisotropy within the ac plane is small, continues to be essentially linear almost down to the ordering temperature. A fit of the polycrystalline average curve above 150 K to the Curie-Weiss law results in an effective moment $\mu_{eff}=4.45 \mu_B/f.u.$ (very close to the expected value of a Yb^{+3} moment) and $\Theta_p=-11.6$ K (indicative of antiferromagnetic coupling).

The upper inset in Fig. 3 details the anisotropic antiferromagnetic transition in the susceptibility $\chi(T)$ at $B=0.1$ T. A peak in $d(\chi T)/dT$ gives $T_N=5.1$ K for this field. The behavior of both curves in the magnetically ordered state is indicative of a nontrivial, and possibly canted, arrangement of the magnetic moments. The upturn at low temperatures for $B \parallel b$ appears to be a genuine response of the compound and not a trivial impurity effect, first, because it does not appear in the $B \perp b$ curve, and second, because it was reproduced almost exactly in two different batches of samples grown with different elemental purities ($3N$ in the first batch and $4N-5N$ in the second.)

The lower inset in Fig. 3 shows magnetic isotherms at 2 K for both directions up to 14 T. There is a spin-flop transition at $B=1.7$ T in the $B \parallel b$ curve. A change in slope near 8 T of both curves marks the crossing of the $T_N(B, T)$ line (a detailed phase diagram will be presented in a future communication), but the magnetization still maintains a positive slope above this transition. If no other metamagnetic transitions are to be found at even higher fields, then it is clear from the graph that the saturated moment at 2 K should remain below $2\mu_B/f.u.$ and therefore significantly smaller than the expected value of $4\mu_B/f.u.$ for saturated Yb^{+3} moments.

In order to shed further light on the ground-state characteristics of YbNiSi₃, the low-temperature, zero-field heat capacity was measured on a Quantum Design PPMS system with ³He option. The open symbols in the inset of Fig. 4 show the measured $C_p(T)$ data below 20 K. A very sharp λ -like peak is seen at $T_N=5.1$ K.

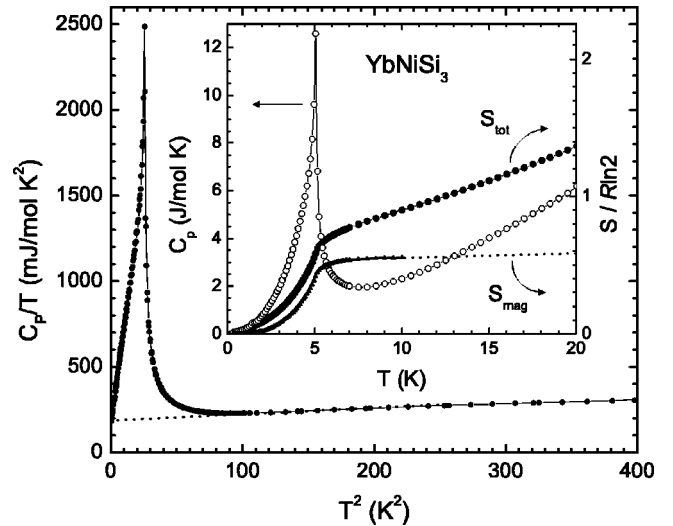


FIG. 4. Zero-field heat capacity measurement on YbNiSi₃ at low temperatures, presented as C_p/T vs T^2 . The dotted line is a linear extrapolation from the 10–20 K region. The inset shows the original C_p vs T data (\circ), the total entropy S_{tot} (\bullet), and the magnetic entropy S_{mag} (\blacktriangle).

The main graph of Fig. 4 shows the same data presented as C_p/T vs T^2 . A linear region is observed between 20 and 10 K, and its extrapolation to $T=0$ (dotted line), coincides with the leveled value of $\gamma=190$ mJ/mol K² that is reached by the lowest-temperature data below 1 K. The coincidence of these two independent estimations gives us confidence in claiming that the obtained value is a good representation of the electronic specific heat, therefore placing it as a moderately heavy-electron system. From the slope of the linear region we obtain the lattice coefficient $\beta=0.26$ mJ/mol K⁴ and estimate the Debye temperature as $\Theta_D=330$ K. We can infer that the first excited CEF levels' energy scale should lie well above 20 K, since no evidence of Schottky anomalies are seen up to this temperature.

In the inset we also present the total entropy $S_{tot}(T)$ (solid symbols) obtained by numerical integration of C_p/T vs T and an evaluation of the magnetic entropy $S_{mag}(T)$, which was obtained by removing the electronic and lattice contributions estimated above from the specific heat before integration. In either case it becomes clear that the total entropy accumulated up to T_N is $\sim 0.6R \ln 2$. Thus, we may conclude that a ground-state doublet is responsible for the magnetic ordering, and the Yb moments are already significantly screened when the magnetic ordering ensues. With the obtained value of γ we can apply Rajan's expression¹⁴ for the specific heat of the Coqblin-Schrieffer model $\gamma T_K \approx 11.2j$ to estimate the Kondo temperature of YbNiSi₃ ($j=1/2$) as $T_K=30$ K.

Finally, we can also use γ , in combination with the previously calculated A coefficient of the Fermi-liquid resistivity model, to estimate $A/\gamma^2=10^{-5} \Omega \text{ cm} (\text{mol K/J})^2$, which is the well-known Kadowaki-Woods ratio, quite commonly observed in heavy fermion systems featuring a ground-state doublet.^{15,16}

In many cases where magnetic ordering coexists with Kondo lattice or heavy fermion behavior, quantitative analysis of the material's low-temperature properties becomes

rather difficult due to the convolution of several contributions to the thermodynamic and transport properties, a problem which can be further aggravated by difficulties in preparation of samples of high quality. The results we have obtained demonstrate that YbNiSi_3 is a welcome exception to the rule and several physical parameters could be quantitatively determined with good accuracy from our measurements. Furthermore, this compound was found to belong to the very rare group of Yb-based materials with magnetic ordering above 5 K, together with YbPtAl ,¹⁷ YbNiSn ,¹⁸ and YbB_2 ,¹⁹ indicating that the intersite indirect magnetic exchange interaction between local moments is strong and dominant, while still displaying very characteristic features of a system with strong on-site Kondo interaction. Therefore, we believe that YbNiSi_3 presents itself as a promising model

system for more in-depth investigations on the delicate balance between these two competing energies, as well as other issues related to Yb compounds and Kondo lattices in general. Studies on the high-field properties and magnetic phase diagram, as well as physical and chemical pressure effects in this compound are currently in progress.

We are thankful to Y. Shibata for the EPMA analysis, to T. Sasakawa for assistance with the XRD refinements, and to F. Iga for his help in the specific-heat measurements. The low-temperature measurements were performed at the Materials Science Center, N-BARD, Hiroshima University. This work was supported by a Grant-in-Aid for Scientific Research (COE Research 13CE2002) of MEXT Japan.

-
- ¹Z. Fisk and M. B. Maple, *J. Alloys Compd.* **183**, 303 (1992).
²P. Haen, P. Lejay, B. Chevalier, B. Lloret, J. Etourneau, and M. Sera, *J. Less-Common Met.* **110**, 321 (1985).
³V. K. Pecharsky, O.-B. Hyun, and K. A. Gschneidner, *Phys. Rev. B* **47**, 11 839 (1993).
⁴H. Yamamoto, M. Ishikawa, K. Hasegawa, and J. Sakurai, *Phys. Rev. B* **52**, 10 136 (1995).
⁵A. Das, L. Menon, A. K. Nigam, and S. K. Malik, *Physica B* **230–232**, 165 (1997).
⁶Y. Muro, D. H. Eom, N. Takeda, and M. Ishikawa, *J. Phys. Soc. Jpn.* **67**, 3601 (1998).
⁷K. Kanai, T. Terashima, D. H. Eom, M. Ishikawa, and S. Shin, *Phys. Rev. B* **60**, R9900 (1999).
⁸A. P. Pikul, D. Kaczorowski, T. Plackowski, A. Czopnik, H. Michor, E. Bauer, G. Hilscher, P. Rogl, and Y. Grin, *Phys. Rev. B* **67**, 224417 (2003).
⁹J. K. Gorelenko, O. I. Bodak, E. I. Gladyshevskii, and V. I. Yarovets, *Ukr. Fiz. Zh. (Russ. Ed.) (Russ. Ed.)* **22**, 1020 (1977).
¹⁰E. I. Gladyshevskii, O. I. Bodak, V. I. Yarovets, J. K. Gorelenko, and R. V. Skolozdra, *Ukr. Fiz. Zh. (Russ. Ed.) (Russ. Ed.)* **23**, 77 (1978).
¹¹P. C. Canfield and Z. Fisk, *Philos. Mag. B* **65**, 1117 (1992).
¹²D. Jaccard and J. Sierro, *Valence Instabilities* (North-Holland, Amsterdam, 1982), p. 409.
¹³K. Alami-Yadri, D. Jaccard, and D. Andreica, *J. Low Temp. Phys.* **114**, 135 (1999).
¹⁴V. T. Rajan, *Phys. Rev. Lett.* **51**, 308 (1983).
¹⁵N. Tsujii, K. Yoshimura, and K. Kosuge, *J. Phys.: Condens. Matter* **15**, 1993 (2003).
¹⁶H. Kontani, *J. Phys. Soc. Jpn.* **73**, 515 (2003).
¹⁷J. Diehl, H. Davideit, S. Klimm, U. Tegel, C. Geibel, F. Steglich, and S. Horn, *Physica B* **206–207**, 344 (1995).
¹⁸K. Drescher, M. M. Abd-Elmeguid, H. Micklitz, and J. P. Sanchez, *Phys. Rev. Lett.* **77**, 3228 (1996).
¹⁹M. A. Avila, S. L. Bud'ko, and P. C. Canfield, *J. Alloys Compd.* **358**, 56 (2003).